PHYSICAL REVIEW D

PARTICLES AND FIELDS

THIRD SERIES, VOLUME 26, NUMBER 1 1 JULY 1982

Diffractive production of vector mesons in muon-proton scattering at 150 and 100 GeV

W. D. Shambroom,* Richard Wilson, B. A. Gordon,† W. A. Loomis, F. M. Pipkin, S. H. Pordes,‡ and L. J. Verhey§
Department of Physics, Harvard University, Cambridge, Massachusetts 02138

H. L. Anderson, R. M. Fine, R. H. Heisterberg,|| H. S. Matis,¶ L. W. Mo,** L. C. Myrianthopoulos, and S. C. Wright
Enrico Fermi Institute, University of Chicago, Chicago, Illinois 60637

W. R. Francis,†† R. G. Hicks,‡‡ and T. B. W. Kirk‡
Department of Physics, University of Illinois, Urbana, Illinois 61801

V. K. Bharadwaj,§§ N. E. Booth, G. I. Kirkbride,|||| T. W. Quirk,¶¶ A. Skuja,*** and W. S. C. Williams
Nuclear Physics Laboratory, University of Oxford, Oxford OX1 3RH, England
(Received 24 August 1981)

We have studied the production of ρ and ϕ mesons from muon scattering on a liquid-hydrogen target at 150 and 100 GeV. For the ρ we observe a skewed mass distribution which becomes somewhat more normal with increasing Q^2 (the square of the four-momentum transferred from the muon), and an exponential distribution in t (the square of the four-momentum transferred to the target proton) with a slope which is consistent with a slight decrease as Q^2 increases. The dependence of the cross section on Q^2 follows that of the square of the ρ propagator with little contribution from longitudinal ρ production. The angular distribution of the ρ decay confirms the smallness of the contribution from longitudinal ρ production at our energies. The cross section when extrapolated to $Q^2=0$ agrees with that measured in real photoproduction. The decay angular distribution of the ρ decay shows that s-channel helicity is largely conserved, although we detect a helicity-single-flip contribution at the 10–15 %-level. Natural-parity exchange in the t channel dominates, and the transverse and longitudinal amplitudes are found to be in phase. These characteristics are consistent with the diffractive nature of the vector-dominance model. The t distribution of ϕ production is also exponential, although less steep than that for the ρ. We observe an elastically produced four-pion state at a mass of approximately 1600 MeV. We identify this state with the $\rho'(1600)$, and find it to be produced with a distribution exponential in t.

I. INTRODUCTION

We present here final results of an experiment measuring vector-meson production from muon-proton scattering at the Fermi National Accelerator Laboratory. We have previously published preliminary results on ρ production.[1]

The vector-meson-dominance model describes the interaction of photons (real and virtual) with matter as proceeding through the coupling of photons to vector mesons which then interact hadronically. Elastic vector-meson production then represents elastic scattering of the virtual vector meson. The vector-meson-dominance idea was first suggested to explain electron-nucleon elastic scattering form factors, which involved a prediction of the existence of vector pion resonances with mass of approximately 600 MeV even before the

first observation of the ρ meson.[2] Although a simple vector-dominance model does not in fact predict the observed dipole form of the nucleon form factors, the pion form factor is more accurately described, and the idea that the photon (real or virtual) couples directly to vector mesons has led to a variety of other successful predictions. Among these is the form of the cross section for photoproduction of vector mesons.[3] The energy dependence, t dependence, and decay angular distribution of this process, as measured in a considerable body of data, encouraged further tests of the vector-dominance approach. To be useful, the model requires the notion that the coupling of a virtual photon to a vector meson be independent of momentum transfer, or at least vary slowly compared to the momentum-transfer dependence of the vector-meson propagator. Values of the ρ photon coupling constant obtained from electron-positron annihilation, photoproduction on heavy nuclei, and comparison of pion photoproduction with production of ρ's by pions are all found to be in reasonably good agreement.

As noted, the vector-dominance approach has been very successful in describing the production of vector mesons by real photons.[4,5]

In leptoproduction of vector mesons we study how the process behaves as the photon becomes spacelike (with mass further from the physical vector-meson mass) and acquires longitudinally polarized components. The vector-dominance theory has been generalized to describe leptoproduction of vector mesons.[6,7]

Several other experiments on ρ leptoproduction have been performed at DESY (Refs. 8–11), at Cornell (Refs. 12–16), and at SLAC (Refs. 17–20).

Several of these experiments use a missing-mass technique, where the scattered lepton and recoil proton are detected. These suffer from a substantial background, and because the ρ-decay pions are not detected, yield no information on the polarization of the ρ meson. Some of the early experiments where the decay pions were detected had such a limited acceptance that they were sensitive only to transverse ρ decays. We will adopt for purposes of comparison results from the DESY streamer-chamber experiment of Joos *et al.*,[11] the SLAC hybrid-bubble-chamber experiment of Ballam *et al.*,[19] the SLAC streamer-chamber experiment of del Papa *et al.*,[20] and the SLAC counter experiment of Dakin *et al.*[18] These experiments span a range in W from 1.7 to 5 GeV. Observation of leptoproduction of ϕ mesons has also been reported.[13,18,14,15,21] An excellent overview of these experiments can be found in the encyclopedic review of Bauer, Spital, Yennie, and Pipkin.[22] In this experiment we extend the range of these investigations to a higher-energy region, with roughly three times the available center-of-mass energy of the previous upper limit. We reasonably expect to be exploring the asymptotic region, safely removed from any influence of low-energy resonances.

We use the following kinematic variables to describe inelastic muon-proton scattering: E, the beam-muon energy; E', the scattered-muon energy; $\nu=E-E'$, the virtual-photon energy; Q^2, the square of the four-momentum transferred from the muon; and W^2, the square of the center-of-mass energy of the virtual-photon–proton system. Description of exclusive vector-meson production requires specification of additional variables: m, the mass of the vector meson; t, the square of the four-momentum transferred to the proton; the azimuthal angle of vector-meson production; and the polar and azimuthal angles of vector-meson decay. Of course, full specification of an event in phase space includes the angles of the incident-muon trajectory, the azimuthal angle of muon scattering in the laboratory, and the spatial position of the interaction vertex. The physics results do not depend on these variables although they must be considered in calculating some corrections.

To compare virtual photoproduction with real photoproduction requires a convention defining the flux of transverse virtual photons. We use that of Hand[23]:

$$\Gamma_T=\frac{\alpha}{8\pi}\frac{W^2-M^2}{E^2M^2Q^2}\frac{1}{1-\epsilon} \tag{1}$$

with transverse polarization of the virtual photon (and the ratio of longitudinal to transverse virtual photons) given by[24]

$$\epsilon=\left[1+\frac{2(Q^2+\nu^2)}{(4EE'-Q^2+Q^2_{\min})}\frac{Q^2}{(Q^2-Q^2_{\min})}\right]^{-1}. \tag{2}$$

The cross section can then be written as

$$\frac{d^2\sigma}{dW^2dQ^2}=\Gamma_T(\sigma_T+\epsilon\sigma_L)\,. \tag{3}$$

Another potentially useful variable is the vector-meson development time. If momentum is conserved in the coupling of the virtual photon to the vector meson, the uncertainty principle allows a time equal to the inverse of the energy difference

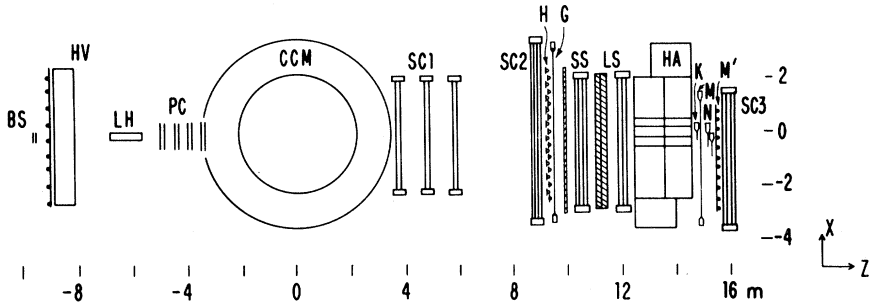

FIG. 1. Plan view of the apparatus. The nominal beam direction is along the $+z$ axis. BS, last beam-tagging station, HV, halo-veto hodoscope and concrete shielding wall; LH, liquid-hydrogen target; PC, multiwire proportional chambers; CCM, Chicago Cyclotron magnet; SC1, SC2, SC3, spark-chamber modules; *H*, *G*, scintillator hodoscopes; SS, steel photon/electron converter wall and spark-chamber module; LS, lead hadron converter and spark-chamber module; *K*, beam veto counters; *M*, *N*, *M'*, muon scintillator hodoscopes.

between the two states for the virtual vector meson to develop. If this development time is less than the typical hadronic size of the vector meson the effect of shrinkage of the interaction radius might be observed as a decrease in the slope of the t distribution.

II. APPARATUS

The muon-scattering facility at the Fermi National Accelerator Laboratory (Fig. 1) has been described in previous publications.[25,26] A tagged beam of muons was focused onto a liquid-hydrogen target 1.2 m long, upstream of a forward spectrometer consisting of ten planes of 1 m$\times$1 m multiwire proportional chambers (MWPC's), the old Chicago Cyclotron Magnet (CCM) modified for use in the apparatus as a spectrometer magnet, twelve planes of 2 m$\times$4 m spark chambers, eight planes of 2 m$\times$6 m spark chambers, and two scintillation-counter hodoscopes. This was followed by two converter and spark-chamber assemblies designed to aid in particle identification, 2.4 m of steel to absorb all particles except muons, three more hodoscopes, and eight planes of 2 m$\times$4 m spark chambers. All told the apparatus comprised 18 multiwire-proportional-chamber planes of over 7000 wires, 58 spark-chamber planes of over 200 000 wires, and 211 scintillation counters.

III. EVENT RECONSTRUCTION

Because of the volume and complexity of the data collected by our apparatus, the transition from raw data to physics results naturally proceeded in many separate stages, taking place at several separate locations and involving several distinct groups of people.

The processing at Oxford of raw data tapes into tertiary tapes containing fitted track has been described in previous publications.[25,26]

Summary tapes were generated for further analysis at Harvard of vector-meson and recoil proton events. It was desired to include all events that were possible vector-meson-event candidates; accordingly, events were selected for these tapes which had any combination of two positive-particle candidates and one negative-particle candidate with momentum totaling less than 1.2 times the beam momentum. This ensured retention of all elastic and inelastic neutral hadronic final states without relying on the preliminary particle identification done at Oxford. Use of this selection program reduced the number of tapes which had to be shipped to Harvard from 60 to 13.

The initial identification of tracks as products of scattered muons or muoproduced hadrons, while adequate for our early publications of inclusive cross sections, was not acceptable for reconstruction of complex multiparticle exclusive final states, where loss of a good particle or inclusion of a halo muon would result in loss of the whole event. The particle-identification problem was therefore attacked from scratch, and a superior algorithm developed. Reconstruction of exclusive states, calculation of various reconstruction corrections, radiative corrections, acceptance corrections, and fitting, followed.

A. Particle identification

The particle tracks reconstructed through the apparatus were produced primarily by the scattered muon, muoproduced hadrons, and halo muons (detected as a result of the long live-times of the spark chambers, and mostly from other rf buckets). To distinguish among these possibilities with the necessary high efficiency a somewhat complex

computer program was developed.

In an initial scan of the track buffer the MWPC track data was revised to take account of the limitations imposed by the location of the interaction vertex, and good quality MWPC and spark-chamber tracks were used to measure fiducial areas and locations of the deadeners in the spark chambers. The scintillation-counter data for each track was revised to reflect the multilayer arrangement of the muon hodoscopes and the uncertainty in counter edge positions, and the number of tracks pointing at each hit counter was accumulated for later use in rating the value (uniqueness) of the counter information. All tracks had their distance at the 6-m chambers in x, u, and v to the nearest other track measured and those separated by less than 12.5 mm in two of the three coordinates were designated as duplicate tracks, although no determination of which track to retain was made at this point. The number of nonduplicated downstream tracks linked to each muon track was counted, again for later use in rating the value of the reconstruction.

Those downstream tracks with at least one link to a MWPC track and one lit counter were considered particle candidates, and subjected to a two-pass examination. These were first tested against several common failure modes: (1) momentum greater than 1.2 times beam momentum, (2) track points within software 6-m-chamber deadener (11 cm in radius, the extra cm to allow for chamber inefficiency near the mylar disc), (3) track points outside software 6-m-chamber fiducial area (5.78 m$\times$2.56 m), (4) momentum vector points outside most downstream MWPC software x limits, (5) number of Chicago chamber sparks less than 3, and (6) total number of sparks less than 11.

Each candidate was then assigned a weight to correct for inefficiency in the track reconstruction. This inefficiency was measured by inserting simulated sparks into real events and analyzing the event normally. The measured inefficiency was parametrized as a function of the x intercept at the 6-m spark chambers, believed to be the relevant parameter.

Quality parameters were assigned to each candidate reflecting the linking to MWPC tracks. A link was considered better if the MWPC track had 4 rather than 2 or 3 points, and if the MWPC track passed close to the overall event interaction vertex. The y position of the downstream track projected to the z position of the overall vertex was checked, and if it was more than 75 mm from the y position of the vertex the quality parameter was decreased.

Data from the G and H hodoscopes were used to determine a downstream timing-quality parameter. Hodoscope elements which fired were said to be hit; those which were pointed at by only one track were called unique; those pointed at by more than one track, shared; and those that were pointed at but did not fire, missed. A track's timing status was evaluated by considering the combined information from all hodoscopes to which it pointed.

The last set of information examined came from the muon chambers and hodoscopes. One parameter reflected links to tracks in the muon chambers, their uniqueness, and the presence of clusters of sparks. In considering the muon hodoscope information the best results from the downstream track itself, projected to those hodoscopes, or the muon track to which it linked (if any), were used. Noting that, due to the muon hodoscope geometry, tracks could point to anywhere from one to four muon hodoscope counters, a quality parameter was determined. These two muon parameters were used in different ways to evaluate each candidate as a possible muon or hadron.

Before determining particle classes the duplicated tracks identified earlier were eliminated. The MWPC and timing-quality parameters were used to discard the lower-quality candidate of each pair according to the following criteria (in order of decreasing priority): (1) failure mode described above (e.g., no surviving MWPC links), (2) MWPC parameter, (3) MWPC x-link parameter, (4) MWPC y-link parameter, and (5) χ^2/spark.

Finally, each candidate was assigned two class ratings, where for muons the class was constrained to be between 1 and 5 and for hadrons the class was constrained to be between 1 and 4. The number of muons of the highest class (usually 1), and the identity of that particle, were duly noted. Eventually, muons up to class 3 and hadrons up to class 2 would be eligible for use in final-state reconstruction.

B. Vertex and associated corrections

The interaction vertex was next calculated using the newly generated information about particle candidate classes. Each linked MWPC track was labeled with the best (numerically lowest) class of the downstream tracks to which it linked. Those linking to a particle candidate of hadron class 2 or better, or muon class equal to the best class muon (if 3 or better), had their previously calculated ver-

tex and error used in a weighted average to determine an overall event vertex, vertex error, and χ^2. This vertex was accepted if the calculated confidence level for the χ^2 obtained was better than 5%. Otherwise, MWPC tracks were discarded one at a time, starting with those of the worst linked class and proceeding in order of decreasing distance from the overall vertex divided by vertex error, and the vertex recalculated. This proceeded until an acceptable χ^2 was reached, and the x and y position of the vertex were computed from the position of the beam track. All momenta were then rescaled to correct for the change in the vertex, and a second pass made through parts of the program: the failure codes (new momenta); the MWPC data (new vertex); and the particle candidate classes (both of the foregoing).

A count was made of unlinked 3 and 4 spark MWPC tracks in x and y coming from the vertex to help in distinguishing inelastic interactions with no downstream hadrons from elastic scatters. For each candidate weights were computed to compensate for the following losses under the assumption that it was a muon, pion, or kaon: (1) track-reconstruction probability, (2) decay upstream of the CCM (would change measured momentum), (3) if not linked uniquely and pointing to the muon-chamber active area, decay between the CCM and the hadron absorber (would cause hadrons to be misidentified as muons), and (4) absorption by material upstream of the CCM, assuming a cross section of 20 mb for pions, 25 mb for kaons.

For each class of hadrons and muons, energy, momentum, and correction weights were summed. Finally, muon and hadron pointers were sequentially arranged in buffers according to class.

C. Neutral-elastic-event reconstruction

Once the particle identification was complete, reconstruction of neutral elastic events began. The quality of the reconstructed beam muon as well as scraping in the last beamline dipole were checked, as were the charge of the scattered muon and the value of the virtual-photon parameters ν, Q^2, and W^2. Hadrons were included in the reconstruction one class at a time in order to make maximal use of the quality distinctions that had been developed. The fraction of successfully reconstructed two-hadron events requiring inclusion of class 2 hadrons was 8.7% at 150 GeV and 14.6% at 100 GeV. The fraction of events reconstructed with class 1 particles where a class 2 particle was present whose inclusion would have spoiled the reconstruction was 0.8% and 0.9%, respectively. For each electrically neutral hadron final state the hadron invariant mass, square of the momentum transfer t, the difference between the square of the undetected recoil-nucleon missing mass, and the square of the target-proton mass were calculated. The calculated difference in the square of the mass is dominated by the difference between the initial- and final-state total energy. The t distribution shows, in addition to a peak at low t, a long high-t tail. The distribution of the square of the mass difference shows an elastic peak and an inelastic background. The elastic peak is seen most cleanly in distributions cut to exclude events with $-t$ greater than 0.8 GeV^2, interaction vertex outside the target, or particle transverse momentum with respect to the pair less than 130 MeV (to exclude e^+e^- pairs) (Fig. 2), although these cuts were not applied at this stage of the analysis. Events were designated as elastic if the absolute value of this difference was less than 7 GeV^2 (approximately corresponding, for small t, to an energy difference between the initial and final states of less than 3.5 GeV).

The "two-hadron" sample actually contained a large number of electron-positron pairs from converted muon bremsstrahlung. These were characterized by their low internal pair transverse momentum and increased propensity to cause showers in the "photon" spark chambers behind

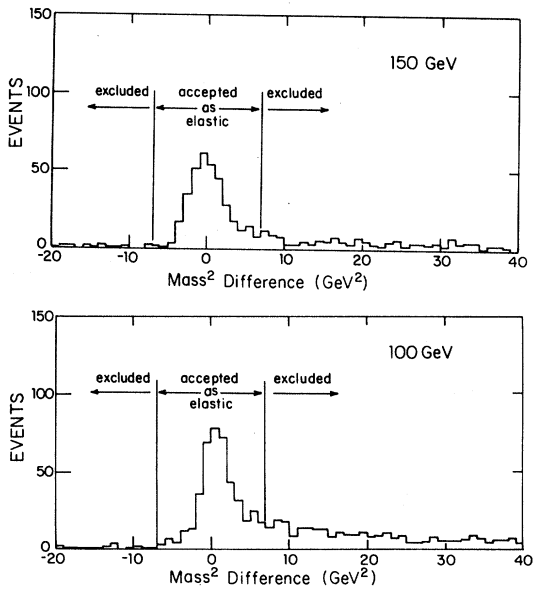

FIG. 2. Difference between the square of the recoil-nucleon missing mass and the square of the proton mass, for two-particle events with $-t$ less than 0.8 GeV^2 passing the vertex cut.

the 5-cm steel converter (SS, Fig. 1), showers which should not penetrate the 16-in. lead hadron converter to the "neutron" spark chambers (LS, Fig. 1). These chambers, however, extended only 4 m in x, were not reliably efficient, and were subject to a fair number of showers produced in the steel by hadrons, and could therefore not be used as a simple electron-positron identifier. They were, however, very useful in developing kinematic cuts to eliminate the electromagnetic events. For each particle, a spark number was defined: $S=$ (number of sparks in "neutron" spark chambers)/6 −(number of sparks in "photon" spark chambers)/8.

Although track finding was not performed on these chambers, this parameter corresponded roughly to the excess of the number of possible tracks in the 6 "neutron" planes over the number of possible tracks in the 8 "photon" planes. The transverse-momentum distribution (Fig. 3) shows enhancements around 360 and 130 MeV corresponding to transverse ρ and ϕ decays, and a peak at low transverse momentum. Examination of the low-transverse-momentum region shows this peak to be at a value corresponding to our experimental resolution (Fig. 4). The criterion finally applied was to exclude events with internal pair transverse momentum less than 80 MeV. The distribution of

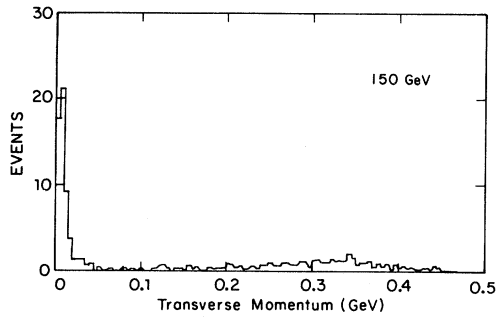

FIG. 3. Transverse momentum of each particle with respect to the pair momentum.

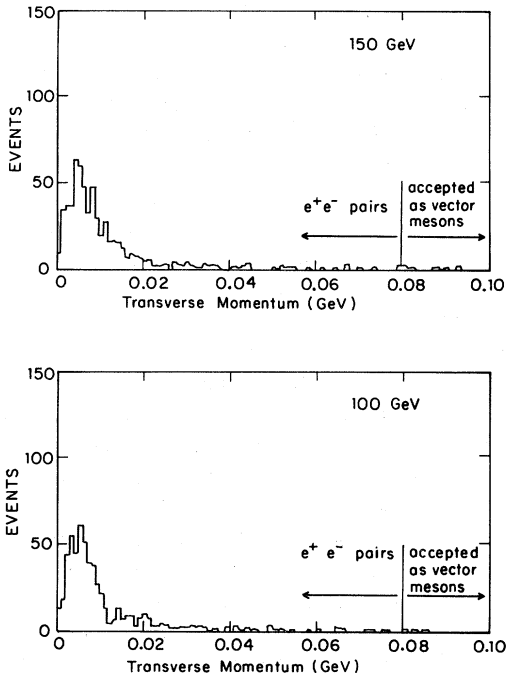

FIG. 4. Transverse momentum of each particle with respect to the pair momentum (low-transverse-momentum region).

the z position of the interaction vertex clearly shows the positions of the hydrogen target and the last beam-tagging hodoscope station, with some indication of the upstream aluminum target flange (Fig. 5). After application of particle class cuts (retaining muons of class 3 or less, hadrons of class 2 or less), vertex cuts (interaction vertex within three standard deviations of the target), and the requirement that the apparatus trigger had been produced by the detected particles, production and decay angles were calculated and relevant variables describing the accepted reconstructed events were written to disk for later access by fitting and mo-

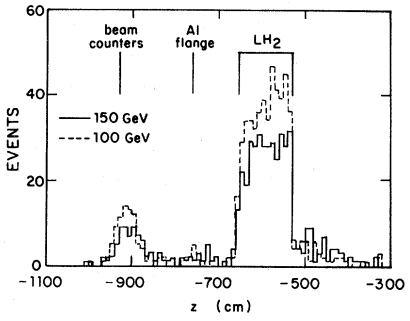

FIG. 5. Z position of the interaction vertex for two-hadron final states.

ment analysis programs.

The mass distribution of these events show a clear and clean ρ signal for the $\pi^+\pi^-$ hypothesis and a ϕ signal for the K^+K^- hypothesis (Figs. 6 and 7). The distributions in t for events in the mass regions of these vector mesons are exponential (Figs. 8 and 9).

IV. CORRECTIONS

Many corrections to the raw numbers of reconstructed events were necessary in order to extract meaningful cross sections. Most were related to inefficiencies in the hardware or software. They fell naturally into three groups: those applied to the data overall, those applied to each event, and those applied to each particle. In some cases the decision of where to apply a correction was based on computational convenience, in others on mathematical rigor.

A. Spark-chamber efficiency

The number of sparks per downstream track was treated as though it obeyed the binomial distribution (which it did to a reasonable approximation), with an average chamber efficiency given by the mean number of sparks per track divided by the number of chambers (20). The average chamber efficiency could thus be obtained by examining all tracks prior to event reconstruction, and used in a summation over the bionomial distribution for 11 or more sparks per track (in accord with our 11 sparks per track requirement). The error on this determination was estimated by relating the binomial probability for 10 sparks per track to the measured standard deviation in the mean number of sparks per track. The results obtained are shown in Table I.

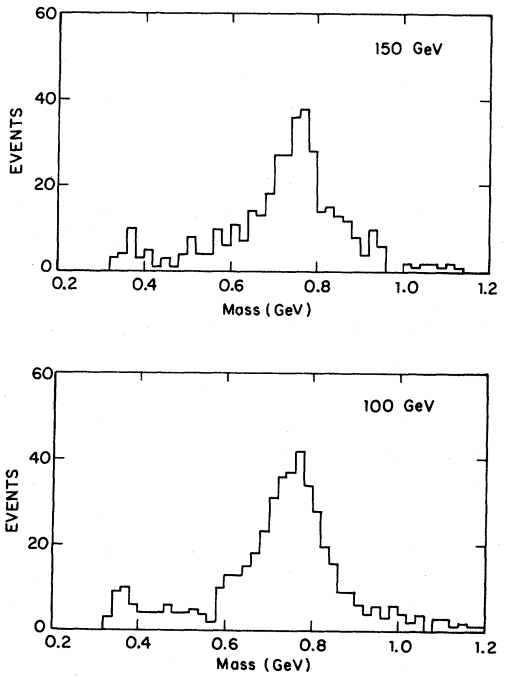

FIG. 6. Invariant mass of two-hadron final states, $\pi^+\pi^-$ hypothesis.

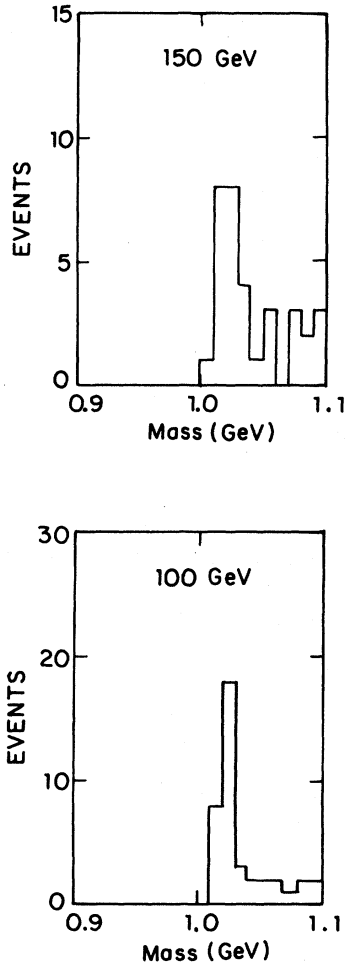

FIG. 7. Invariant mass of two-hadron final states, K^+K^- hypothesis. Note that plot is truncated at the high-mass end.

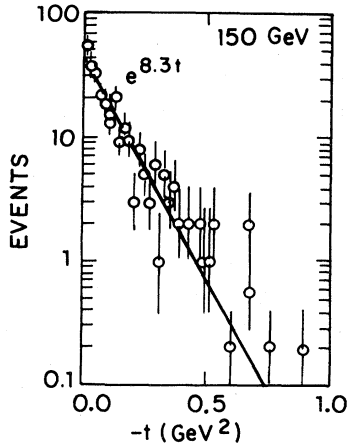

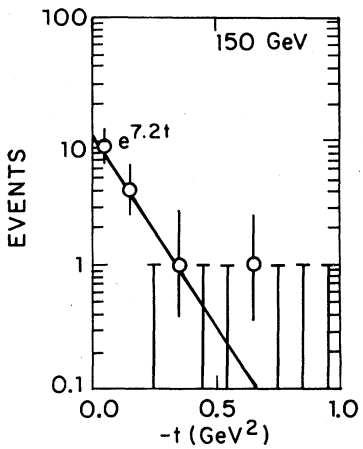

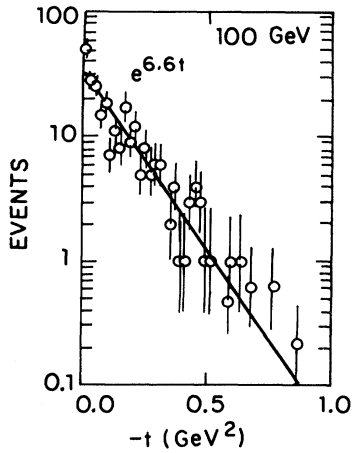

FIG. 8. Uncorrected t distribution for events with pion-pair mass in the range 500 to 1000 MeV.

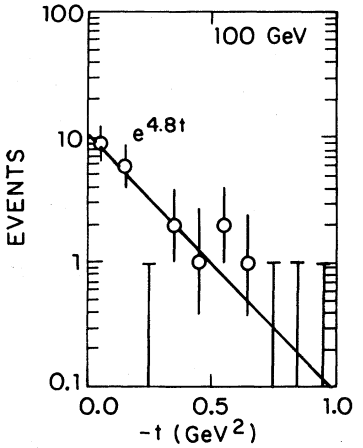

FIG. 9. Uncorrected t distribution for events with kaon-pair mass in the range 1000 to 1040 MeV.

B. Particle-reconstruction efficiency

The efficiency of the apparatus as used in the event-reconstruction procedure was measured using particles from successfully reconstructed events. In considering each section of the apparatus (MWPC's, downstream hodoscopes, and muon chambers and hodoscopes), particles with highest quality information in the other two sections were used to determine the distributions in quality variables for presumed good particles. Negative and positive particles were treated separately, as were hadrons and muons in the muon chamber and hodoscope section. The products of probabilities were then summed over all combinations which would yield acceptable reconstruction (class 1 or 2 for hadrons, class 1, 2, or 3 for muons). The overall reconstruction efficiencies are shown in Table II.

TABLE I. Spark-chamber efficiency.

	150 GeV	100 GeV
Mean number of sparks per track	14.8±3.0	14.3±3.3
Average chamber efficiency	0.74	0.72
Single-track efficiency (> 10 sparks)	0.98	0.97

The slightly lower efficiency for positive hadrons is primarily due to the fact that these particles more often shared lit counters (with the muon), and were therefore less easily recovered from the effects of inefficiencies elsewhere. The 100-GeV efficiency was lowered with respect to the 150-GeV efficiency primarily by inefficiencies in the G hodoscope. (These efficiencies can be compared

TABLE II. Overall reconstruction efficiency.

	150 GeV	100 GeV
Negative hadrons	0.996±0.002	0.987±0.003
Positive hadrons	0.985±0.004	0.978±0.005
Muons	0.994±0.002	0.991±0.003
Three particles	0.975±0.005	0.957±0.007

with those obtained from the simpler uncorrelated reconstruction requirements of an x MWPC link, each counter pointed at being lit, and a unique track link or lit counter for the muon. The three-particle reconstruction efficiency would have been 0.893 for the 150-GeV data and 0.719 for the 100-GeV data.) Halo muons could randomly link to MWPC tracks and point to lit counters. Such excess particles from successfully reconstructed events were studied to determine the probability of a halo muon achieving class 1, and thereby spoiling the reconstruction. This probability was measured to be 0.001 for the 150-GeV data and 0.002 for the 100-GeV data.

C. MWPC efficiency

An additional correction had to be applied for downstream particle tracks with no MWPC links, as these would not be considered as particle candidates. The inefficiencies found are shown in Table III. The three-particle inefficiencies of 0.2% and 0.3% were ignored.

This procedure could correct only for random, uncorrelated inefficiencies. In particular, failure of the entire MWPC system (such as would occur in the event of a malfunction of the high-voltage ramping system) would go undetected here. Imbedded beam events were therefore used to search for an excess of simultaneous x and y failures over the number predicted by x and y failures independently. (It should be noted that the MWPC inefficiency for beam events is expected to be higher than that for normal trigger events because the beam tracks populate a smaller area of the MWPC's and are parallel, allowing pre-amp dead time to have a greater effect.) The beam-to-MWPC linking requirement, applied at the MWPC center of measurement, was that the intercept and slope differences lie within an ellipse of radii given by the calculated intercept and slope errors. The inefficiencies seen are shown in Table IV. No excess inefficiency was seen.

TABLE III. MWPC inefficiencies (uncorrelated).

	150 GeV	100 GeV
Negative particles		
No x link	0.018±0.004	0.026±0.005
No y link	0.032±0.005	0.040±0.006
Positive particles		
No x link	0.022±0.004	0.029±0.004
No y link	0.035±0.005	0.035±0.004

D. On the matter of bad runs

Efficiencies of various parts of the apparatus varied over the course of data taking, and corrections were applied to compensate for these inefficiencies. As a check, the vector-meson reconstruction was run excluding runs which met one of two criteria:

(1) Mean number of sparks on all found tracks was less than 11.

(2) Inefficiency in any hodoscope (as measured by particles from reconstructed vector-meson events with best-quality MWPC information and uniquely lit counters in the hodoscopes not being considered) nonzero by more than two standard deviations.

For the 100-GeV data this excluded 14 runs representing 20% of the total beam. The number of reconstructed ρ mesons per 10^9 beam muons, corrected for spark-chamber efficiency, was found to be 26.9±1.4 for the 58 good runs and 27.0±1.2 for all 72 runs. The difference is found to be accurately corrected for by the spark-chamber efficiency correction. All runs were therefore retained.

E. Inelastic contamination

The correction for inclusion of nonelastic pion and kaon pairs was determined by considering the

TABLE IV. MWPC inefficiencies (correlated).

	150 GeV	100 GeV
No x link	0.210±0.005	0.165±0.006
No y link	0.165±0.005	0.148±0.006
No x or y link		
Predicted	0.035±0.001	0.024±0.001
Measured	0.036±0.002	0.023±0.003

distribution of events as a function of the square of the recoil-nucleon missing mass, for those events with $-t$ less than 0.8 GeV^2, internal pair transverse momentum greater than 130 MeV, and interaction vertex in the target (Fig. 2). Two types of background are apparent. The roughly constant low-level noise signal at unphysical negative mass^2 is likely due to mislocation of the vertex in multivertex events (e.g., converted bremsstrahlung) and MWPC inefficiencies. It is assumed to be constant under the peak, and amounts to $(6\pm2)\%$ at 150 GeV and $(5\pm1)\%$ at 100 GeV. The slightly sloping shoulder at positive-mass^2 values is due to inelastically produced states where only two hadrons (the detected neutral pair) successfully transverse the CCM field. This contribution to the distribution, which must go to zero at a mass^2 difference of zero, appears to peak between 10 and 20 GeV.[2] The distribution in the region between 10 and 40 GeV^2 was fit with a function of the form

$$y = a\sqrt{x} + bx \ . \tag{4}$$

This form goes to zero at zero mass difference, but otherwise is purely empirical. Integration of the fitted curve gave a fractional inelastic contamination of $(9\pm2)\%$ at 150 GeV, and $(12\pm2)\%$ at 100 GeV. The higher inelastic rate for the 100-GeV data is expected because that data set contained a higher proportion of data at high Q^2 where elastic production is expected to be suppressed. This calculation was checked by assuming that the inelastic contribution achieved its average level over the 10–20 GeV^2 range at 10 GeV^2, and went linearly to zero at 0 GeV^2, with an error estimated by assuming the probability of a given level of contamination was uniform between zero and twice the measured level. This alternative approach yielded a contamination estimate of $(5\pm3)\%$ at 150 GeV and $(9\pm5)\%$ at 100 GeV, consistent with the previous method.

F. Beam-reconstruction efficiency

To avoid the problems caused by biasing of the beam distribution by the event-trigger requirement, the beam-reconstruction efficiency was measured using events triggered by the beam only, taken every 4×10^6 beam muons. The efficiency was found to be $(73.0\pm0.6)\%$ at 150 GeV and $(73.8\pm0.6)\%$ at 100 GeV.

G. Multiple-muon vetoing

Beam muons in rf buckets with another muon were effectively disabled from triggering the apparatus, for even if they scattered, the other muon was overwhelmingly likely not to, and would hit the K beam veto. To reduce the fraction of beam suffering from this effect, a requirement was included in the trigger that not more than one counter be hit in each of the last five beam-triggering stations. To measure the residual contamination the muon-tagging counters hit for each reconstructed event were compared to those for the previous event; the resulting fraction was multiplied by a delayed coincidence rate equivalent to the fraction of rf buckets containing multiple muons. The resultant correction was less than 0.1%, and was ignored.

H. Empty-target fraction

The presence of a signal on the downstream side of the target in the vertex z distribution suggests the need for an empirical empty-target subtraction. Empty-target data was taken with approximately one tenth the beam used on the full target. Stability of the various reconstruction corrections for the empty-target runs can be checked by the empty-target fraction for events originating in the last beam-tagging hodoscope station, which did not change during target-empty running. We find empty to full rate ratios of 0.95 ± 0.36 at 150 GeV and 1.32 ± 0.37 at 100 GeV, consistent within errors with unity. The measured empty-target fractions for the hydrogen target are $(17\pm6)\%$ at 150 GeV and $(20\pm6)\%$ at 100 GeV. The Mylar target vessel, downstream aluminum can end, and cloth target hood contributed a fraction of 4% in g/cm^2 and 9% in radiation lengths. There is clearly another source of background, and a measured rather than calculated correction is necessary.

I. Veto-shower correction

The scattered muon emerging from the steel hadron absorber was sometimes accompanied by an electromagnetic shower. If the muon passed close enough to the veto, these particles could hit it even if the muon itself missed it. The distribution of such showers was studied by examining the central muon hodoscope data for imbedded beam triggers; its overlapped counters gave spatial information in

3.8-cm bins. The maximum extent of these showers was found to be best fit by an exponential with an overall shower probability of 24% and a spatial distribution exponential constant of 6.50 cm at the muon hodoscope, implying a constant of 2.25 cm at the unscattered beam veto, which was closer to the steel. Accordingly, for each event a weight was calculated based on the distance of the muon in x and y from the veto.

J. Acceptance and radiative corrections

For efficiency, the Monte Carlo program used the method of importance sampling.[27] The sampling distribution used was uniform in all nonbeam kinematic and spatial variables save three: (1) In Q^2 the distribution fell as Q^{-2} for Q^2 less than the square of the vector-meson mass, and Q^{-6} for Q^2 greater than the square of the vector-meson mass; this approximates the product of the virtual-photon flux and vector-meson propagator. (2) The distribution in the square of the vector-meson mass was a constant-width Breit-Wigner form. (3) In t, the distribution was exponential. Events were appropriately weighted to recover the exact form of the cross section being simulated. Because we are interested in extracting virtual-photon cross sections (with the virtual-photon flux factor divided out), the acceptance integration used as a weighting factor the virtual-photon cross section.

The system was used in a mode that produced radiative and acceptance corrections on an event-by-event basis, useful and appropriate for the maximum likelihood and moment analyses employed. The record of kinematic data written by the reconstruction program was read in, and four separate integrations were performed, assuming separately that the event was a pion pair or a kaon pair. The data were considered in bins of W^2 and Q^2; the bin in which the event fell was determined, and the limits of that bin used at the limits of integration for those variables. For one pair of integrations the mass and t were held fixed and the angles integrated over under the assumption of s-channel helicity conservation, with a small (ξ^2 equal to 0.1) longitudinal contribution. Next, the angles were held fixed and the mass and t integrated over, assuming a modified relativistic Breit-Wigner mass spectrum and t slope of 8 GeV^{-2} for the ρ, and a simple Breit-Wigner and t slope of 5 GeV^{-2} for the ϕ. In all four integrations the beam and scattered muon variables and interaction vertex were integrated over. Data from imbedded beam triggers were used to simulate the beam.

After propagating the simulated particles through the apparatus to determine if a trigger would occur and which particles would be detected (being mindful of the muon hodoscope geometry, two out-of-trigger G counters, spark-chamber deadeners, and other details), a program functionally identical to that used on the real data was employed to reconstruct the event. This procedure provided a check on possible idiosyncrasies in the reconstruction program (none were found) and allowed a measurement of the effects of hardware and computational resolutions (which were found to be negligibly small). The radiative correction integration was performed using the prescription of Urban.[28] Each event record, along with its corrections, was written back to disk.

One hundred points were used for each of the four integrations for each event, assuring that the uncertainty in these calculations would be approximately 10% of the statistical uncertainty inherent in the data. This procedure required 45 sec of VAX 11/780 time per event.

An approximate but intuitive check can be made on the dominating muon part of the radiative corrections with the virtual-radiator approximation, whereby the interaction is preceded and followed by a virtual radiator whose thickness in radiation lengths is[29]

$$\frac{3}{4}\frac{\alpha}{\pi}\left[\ln\left[\frac{Q^2}{m^2}\right]-1\right]. \tag{5}$$

The minimum radiated photon energy is set at approximately 3.5 GeV by our cut in the square of the recoil-nucleon missing mass; the maximum is approximately fixed by the beam-muon energy. The radiation probability was integrated to lowest order in photon energy k. We compare results (in percent) from this formula (VR) with values roughly interpolated from Monte Carlo (MC) output in Table V. The agreement is excellent, and gives confidence in the rigorous procedure. (We note here that our earlier publication[1] used an incorrect parametrization of Urban's prescription giving larger values for this correction, although not enough to affect the final results.)

K. Corrections applied to each particle

Each particle was weighted to correct for losses from three sources. The efficiency of the track finder was found to vary as a function of x posi-

TABLE V. Comparison of radiative corrections as calculated by virtual-radiator approximation (VR) and Monte Carlo integration (MC).

Q^2 (GeV^2)	150 GeV VR	150 GeV MC	100 GeV VR	100 GeV MC
0.1	1.7	1.6	1.5	0.9
0.3	3.1	3.4	2.8	2.0
0.8	4.4	4.5	4.0	3.5
3.0	6.2	6.6	5.5	5.1

tion at the 6-m chambers due to confusion caused by sparks from stale beam tracks. This inefficiency was measured in a separate procedure whereby simulated sparks were inserted into real events which were then analyzed. Pions and kaons which decayed upstream of the CCM would have measured momenta differing from their original momentum, while those pointing at the muon chambers which decayed into muons before the hadron absorber would reconstruct as muons. Pions and kaons which rescattered in the material upstream of the CCM would likewise fail to reconstruct. In estimating this effect a cross section of 25 mb for pions and 20 mb for kaons was assumed. The foregoing correction weights were computed as part of the particle identification procedure.

L. Corrections summary

The total luminosity was adjusted by the corrections applied to the data overall, shown in Table VI; the values for the variable corrections, applied during event reconstruction, are also included for reference.

V. RESULTS

A. Mass- and t-distribution fits

The ρ mass spectrum in photoproduction and leptoproduction is known to be skewed, presumably due to the interference of nonresonant dipion

TABLE VI. Corrections summary.

Corrections applied to data overall (percent)	150 GeV	100 GeV
Spark-chamber efficiency	5.3 ±0.1	10.9 ±0.1
Particle-reconstruction efficiency	2.6 ±0.5	4.5 ±0.7
Inelastic contamination	11 ±3	14 ±5
Beam-reconstruction efficiency	37.0 ±1.1	35.5 ±1.1
Empty target	17 ±6	−20 ±6
Final overall correction factors		
ρ	1.27 ±0.10	1.25 ±0.12
Unobserved ϕ-decay modes	2.058	2.058
ϕ	2.61 ±0.20	2.57 ±0.25
Range and average value of variable corrections (percent)	**150 GeV**	**100 GeV**
Each event:		
Veto shower	0−31.6,0.3	0−31.6,0.4
Radiative corrections	0.8−6.6,1.8	0.4−5.1,1.6
Each particle:		
Track-finding efficiency	0−20.5,3.1	0−20.5,3.0
Pion decay	0−3.0,0.8	0−4.8,1.3
Kaon decay	0−18.3,4.9	0−30.0,11.9
Pion rescattering	1.6−16.3,8.7	1.6−16.3,8.8
Kaon rescattering	1.2−12.8,6.9	1.2−12.8,7.0

production with the ρ resonance. Various formulations are used to describe the deviation of the dipion mass spectrum from a pure relativistic Breit-Wigner distribution, including the Soding model[30] and mass-skewing factors, with or without t or Q^2 dependence.[31]

This experiment produced a very clean ρ signal, with little discernible background, and in addition the presence of a ϕ signal and the absence of particle identification required use of the maximum likelihood method for determining mass distribution parameters. A parametrization in common use, a relativistic Breit-Wigner distribution multiplied by a skewing function with variable exponent, was used to determine the ρ to ϕ ratio in our data. This had the advantage of yielding normalized distributions which were inherently positive at all mass values. The cross sections were evaluated at the resonance peak, such that the results are largely model independent, contributions from nonresonant background are expected to cancel, and comparison between different experiments is facilitated.[32]

The basic form for a spin-1 object decaying into two spin-0 objects is given by a relativistic Breit-Wigner with energy-dependent width[33]

$$F=\frac{2}{\pi}\frac{mm_0\Gamma}{(m^2-m_0^2)^2+m_0^2\Gamma^2},$$
$$\Gamma=\Gamma_0\left[\frac{q}{q_0}\right]^3\frac{m_0}{m}, \tag{6}$$
$$q=\frac{(m^2-4m_\pi^2)^{1/2}}{2},\quad q_0=\frac{(m_0^2-4m_\pi^2)^{1/2}}{2},$$

where q is the decay particle momentum in the center of mass.

We take for the observed two-pion mass spectrum this basic form multiplied by a mass-skewing factor with variable exponent. As the width of the ϕ is less than our apparatus resolution, the ϕ peak appears as a Gaussian mass distribution, modified by the transverse-momentum cutoff. Thus we use for the overall mass and t distribution

$$(1-a)\left[\frac{m_0}{m}\right]^n F(m_{\pi\pi})e^{-b|t|}+aG(m_{KK})e^{-c|t|}. \tag{7}$$

Parameters of the vector-meson mass and t distributions were determined by the maximum likelihood method. Since each event was subject to two hypotheses, that of being a pion pair and that of being a kaon pair, and consequently had two possible invariant masses, a procedure involving curve fitting to binned data was not possible. The maximum likelihood approach is a powerful means for estimating parameters of multidimensional distributions which is unbiased and makes maximal use of the data; no information is lost through binning. For each bin in W^2 and Q^2 the negative-logarithmic-likelihood function was minimized using the program MINUIT. The maximum-likelihood method requires that values of corrections which depend on the kinematic variables the distributions of which are being measured be available for each event, in particular radiative corrections and acceptance. Accordingly, the Monte Carlo acceptance system was used in a mode whereby each event was read in, and with mass and t held fixed, acceptance and radiative corrections were integrated over all other variables, for both the two-pion and two-kaon hypotheses. An initial fit was made for data in the region of W^2 where the data extend to Q^2 of zero to determine the measured mass, mass resolution, and t-distribution slope for ϕ. We obtained ϕ mass values of 1022 ± 2 and 1021 ± 2 MeV, mass resolutions of 7 ± 2 and 6 ± 1 MeV, and t slopes of 7.2 ± 1.7 and 4.8 ± 1.2 GeV^{-2} at 150 and 100 GeV. (The ϕ t-distribution slope was found by Dixon *et al.*[21] to range between 3.1 ± 0.4 and 4.0 ± 0.2 for Q^2 between 0.125 and 1.3 GeV^2 at W of 2.9 GeV. Our observation of somewhat steeper slopes is possibly due to contamination of our sample by e^+e^- events.) These parameters were then held fixed for determinations over individual W^2Q^2 bins of the ϕ-to-ρ relative cross sections and the ρ-mass- and t-distribution parameters.

The results obtained for the ρ-mass-skewing parameter are presented as a function of Q^2 in Fig. 10. Some previous experiments have observed a decrease in the skewing of the ρ mass spectrum with increasing Q^2, while others have found the skewing to be essentially constant. If our results are parametrized as a linear function of Q^2 we obtain

$$n=(3.65\pm0.22)-(0.37\pm0.33)Q^2 \tag{8}$$

(Q^2 in GeV^2) with a χ^2 of 15.6 for 9 degrees of freedom. Our results favor a moderate falloff in the amount of skewing, somewhere between the extremes found by previous workers.

Figure 11 shows the exponential t-distribution slopes obtained for the ρ. If our data alone are fit to a simple function linear in Q^2 we obtain the result

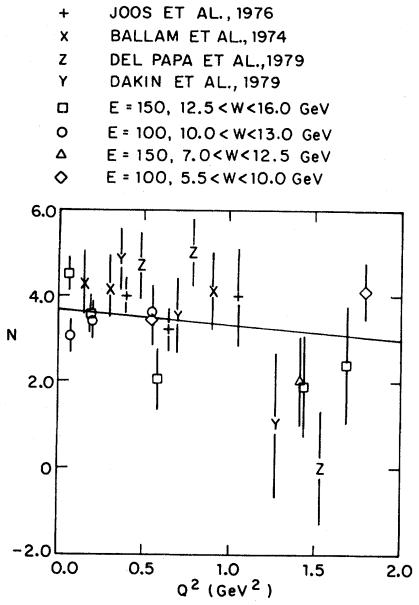

FIG. 10. Skewing parameter for the ρ mass distribution. The line is a fit to our data.

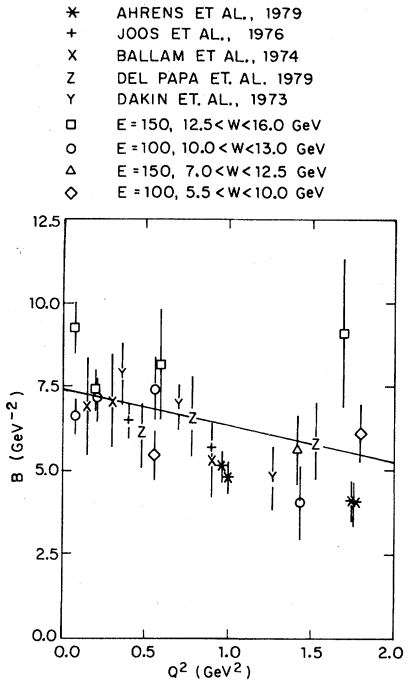

FIG. 11. Slope parameter of the ρ exponential t distribution. The line is a fit to our data.

$$B=(7.40\pm0.34)-(1.09\pm0.44)Q^2 \qquad (9)$$

(B in GeV)$^{-2}$, Q^2 in GeV^2) with a χ^2 of 18.0 for 9 degrees of freedom. Taken all together, the world data suggest a slope decreasing as Q^2 increases, and are consistent with our results, with the exception of the points from Ahrens *et al.*,[16] which are low. Considering the slope to be a function of development time is not illuminating. Our data, spanning development times from 14 to 400 GeV^{-1}, show a decrease with increasing Q^2 similar to the earlier data in the development time range from 4 to 14 GeV^{-1}. In an optical model this slope reflects the effective interaction radius of the virtual photon and proton. In this description the slope should decrease with increasing Q^2 if the virtual photon becomes more pointlike (photon shrinkage).

B. Q^2 dependence of the cross section

Vector dominance, along with the assumption that longitudinal and transverse production have the same t dependence, predicts for the Q^2 dependence of the ρ cross section the form

$$\sigma(Q^2)=\sigma(0)\left[\frac{m^2}{m^2+Q^2}\right]^2\left[1+\epsilon\xi^2\frac{Q^2}{m^2}\right], \qquad (10)$$

where factors correcting for variation in photon flux and minimum t, which are negligible at our energies, are neglected. The second factor is the square of the virtual-ρ propagator. The parameter ξ in the final factor, which accounts for longitudinal ρ production, is the ratio of longitudinal to transverse forward amplitudes, which by the optical theorem equals the ratio of the longitudinal and transverse total cross sections if the amplitudes are predominantly imaginary (as is the case for diffractive processes). To determine the two free parameters, the cross section at $Q^2=0$ and ξ^2, the mass and t fitting routine evaluated the integral over each Q^2W^2 bin of the cross section divided by the square of the ρ propagator. This quantity is then plotted as a linear function of the virtual-photon polarization times $Q^2/m_0{}^2$. Linear least-squares fits then yield, from W^2 regions where our data extend to Q^2 of zero, an extrapolated real-photon cross section of 9.67 ± 0.72 μb at 109 GeV and $7.96+0.63$ μb at 72 GeV, with ξ^2 values of 0.06 ± 0.19 and 0.11 ± 0.17. Our results thus show no important contribution from longitudinal ρ production. This is consistent with our measurement of the decay angular distribution, and thus is different from the interpretation of experiments done

at lower energies by del Papa *et al.*[20] Figure 12 shows a familiar plot of the cross section as a function of Q^2, along with the Q^2 dependence expected from the square of the ρ propagator normalized to both the 150- and 100-GeV data. The cross section extrapolated to $Q^2=0$ is directly comparable to that measured in real photoproduction. Figure 13 compares our results with those from a recent high-energy photoproduction experiment,[34] along with an extrapolation of early data from this experiment.[1] The agreement is excellent.

We measure an overall ratio of ϕ to ρ production of 0.07 ± 0.01 at 150 GeV and 0.13 ± 0.02 at 100 GeV. The errors quoted are statistical; the systematic uncertainty due to possible contamination by high-transverse-momentum e^+e^- pairs advises caution in accepting these results. Comparison with measurements at lower energies is not meaningful, as high-energy photoproduction measurements, as well as theoretical predictions based on vector dominance plus an additive quark model, show the photoproduction cross section to be rising with energy. We lack sufficient statistics to measure the Q^2 dependence of the ϕ muoproduction cross section, and thus cannot resolve the contributions to our overall result from the cross section at $Q^2=0$ and the Q^2 dependence. Other experiments have shown the Q^2 dependence of ϕ production[21] and ψ production[35] to be given by the square of their respective propagators.

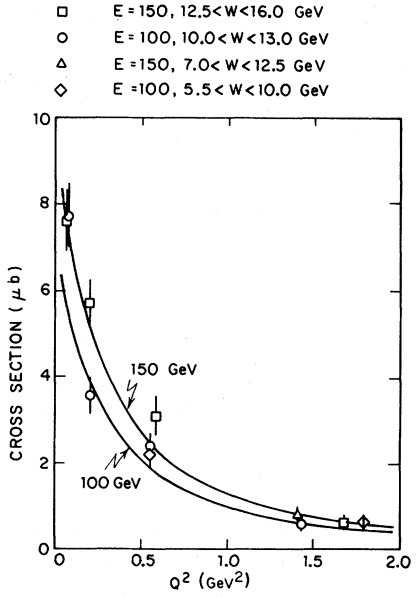

FIG. 12. Cross section for ρ virtual photoproduction as a function of Q^2. The lines show the Q^2 dependence expected from the square of the ρ propagator.

C. ρ-decay angular distribution

The angles used to describe the ρ production and decay are specified in the s-channel helicity system. In the center-of-mass system of the $\rho+$ recoil proton the azimuthal angle of the virtual-photon polarization vector is given by the angle Φ between the normals to the ρ-production plane and the muon-scattering plane. The ρ-decay azimuthal angle is given by the angle ϕ between the normals to the ρ-production and the ρ-decay planes in similar fashion. We define the difference angle

$$\psi=\Phi-\phi\ . \tag{11}$$

The pion polar decay angle in the ρ center-of-mass system with respect to the ρ direction is given in the ρ center-of-mass system by θ. This is illustrated in Fig. 14.

The angular distribution of the ρ decay is analyzed in terms of the ρ spin-density matrix in the helicity system.[24]

For ρ mesons produced by a longitudinally polarized muon beam the density matrix can be decomposed into nine orthogonal Hermitian 3×3 matrices, where the matrices $0-3$ describe production by transverse protons (0 unpolarized, 1 and 2 linear polarization, 3 circular polarization), 4 describes production by longitudinal photons, and $5-8$ describe transverse-longitudinal interference terms. The contributions from 3, 7, and 8 depend on the muon-beam polarization. If the longitudinal-to-transverse ratio R is not determined by

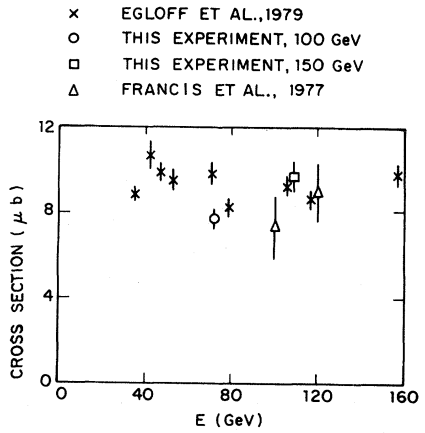

FIG. 13. ρ-photoproduction cross section, including results of this experiment extrapolated to $Q^2=0$.

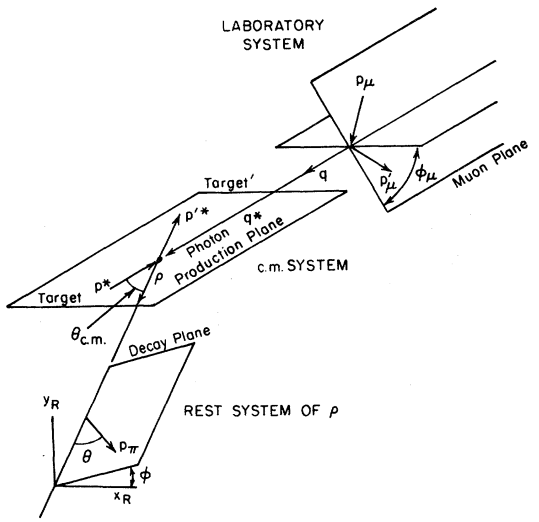

FIG. 14. Angles used to describe ρ production and decay.

measurements at different virutal-photon polarizations for fixed W^2 and Q^2 (i.e., different beam energies) the ρ-decay angular distribution measures elements of combination matrices which are linear combinations of the density matrices.

The most general ρ-decay angular distribution is written in terms of 23 real and imaginary parts of elements from these combination matrices. The elements can be determined from our data by the method of moments. Events with pion-pair masses in the range 500 to 1000 MeV were used with each event weighted to correct for acceptance as a function of angles, in addition to the usual event-by-event corrections. In determining the various parameters derivable from the density-matrix elements no constraints were applied. Obviously, the physics places limitations on the true values; R cannot be negative, the absolute value of the cosine of the angle between the transverse and longitudinal amplitudes cannot exceed one, nor can the parity asymmetry. When the values determined from measurements exceed these limits it can be regarded as implying consistency with the limiting value to the extent implied by the stated errors, or perhaps as a test of the validity of the parametrization being discussed. Some other workers have constrained their results, and we cannot determine from their results alone whether this was done by an *ad hoc* adjustment of reported values or quoted errors, or by some more complicated procedure.

If s-channel helicity conservation (SCHC) holds, all elements save seven are zero, and three constraint equations apply to another six elements. Comparing our data with the assumption that s-channel helicity is conserved yields an overall χ^2 of 17.2 at 150 GeV and 20.0 at 100 GeV, for 19 degrees of freedom for the ρ. (But note the small single-flip contribution discussed later.)

The assumption of SCHC reduces the number of independent helicity amplitudes to three. We can consider ρ production to proceed via exchange in the t channel of systems with pure natural parity [natural-parity exchange (NPE)] or pure unnatural parity. If the assumption that only natural parity $[P=(-1)^J]$ is being exchanged is added to that of SCHC there remain only two independent amplitudes. If their relative phase is defined as δ the decay angular distribution reduced to the form

$$W(\cos\theta,\Psi)=\frac{1}{1+\epsilon R}\frac{3}{8\pi}\{\sin^2\theta(1+\epsilon\cos^2\Psi)+2\epsilon R\cos^2\theta-[2\epsilon(1+\epsilon)R]^{1/2}\cos\delta\sin^2\theta\cos\Psi$$
$$+[2\epsilon(1-\epsilon)R]^{1/2}P\sin\delta\sin^2\theta\sin\Psi\}\ , \tag{12}$$

where P is the muon-beam polarization.

We can extract from the measured matrix elements, assuming SCHC and NPE, values for R and $\cos\delta$ (Figs. 15 and 16). R can be expressed in the form

$$R=\xi^2Q^2/m^2\ , \tag{13}$$

where m is the ρ mass, and ξ^2 is the square of the ratio of longitudinal-to-transverse total ρ-nucleon cross sections. This parametrization meets the obvious requirement of going to zero at $Q^2=0$. Fitting our results for regions of W^2 where data extends to $Q^2=0$ yields, for the parameter ξ^2, -0.07 ± 0.15 at 150 GeV and 0.21 ± 0.16 at 100 GeV, consistent with zero. Previous experiments at lower energies have found an increase in R as Q^2 increases. In Fig. 17 we plot values of R from several experiments for Q^2 between 1.0 and 1.5 GeV^2 as a function of energy. We note that R decreases with increasing energy, becoming consistent with zero.

If we neglect products of two helicity-flip ampli-

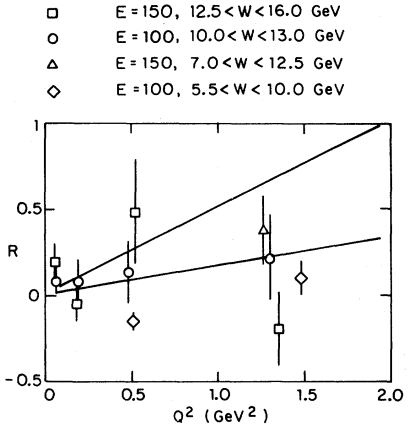

FIG. 15. The ratio of longitudinal to transverse ρ production. The lines indicate the Q dependence expected for $\xi^2=0.1$ and $\xi^2=0.3$ (see text).

tudes, assume that the helicity-flip and helicity-nonflip amplitudes are in phase, and further assume that the ratios of helicity-single-flip to helicity-nonflip amplitudes are the same for transverse and longitudinal photons[11] then we can estimate the magnitude of the helicity-single-flip contribution (Fig. 18). We find an overall contribution of $(14\pm8)\%$ at 150 GeV and $(11\pm8)\%$ at 100 GeV. This is of course a small but specific violation of SCHC. Joos *et al.*[11] found a single-flip contribution of 15—20% for W between 2.1 and 2.8 GeV; we find that the effect persists at our energies, although we are well removed from the effects of the resonance region.

We can test the dominance of natural-parity exchange for transverse photons by computing the

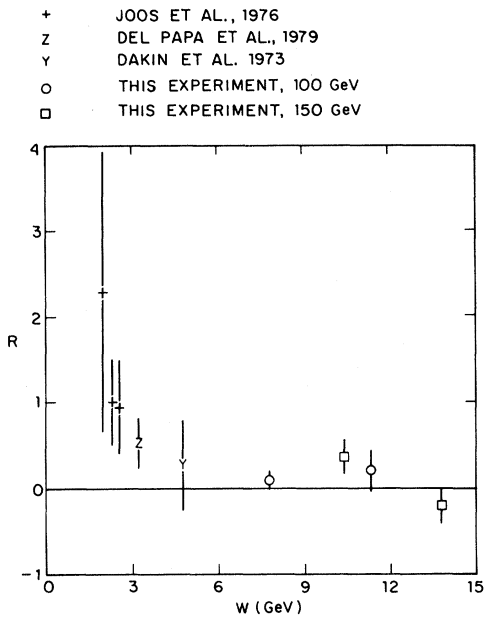

FIG. 17. Energy dependence of the ratio of longitudinal to transverse ρ production for Q^2 between 1.0 and 1.5 GeV^2.

parity asymmetry parameter P (Fig. 19). This requires finding moments of terms with the virtual-photon polarization parameter in the denominator, and thus is not reliable at low Q^2 where the virtual-photon polarization goes to zero.

Tables VII and VIII give the density-matrix elements, as well as several quantities derived from them, measured over the kinematic region where our acceptance extends to $Q^2=0$.

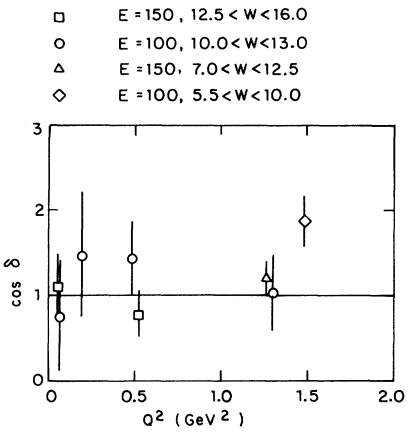

FIG. 16. Cosine of the angle between longitudinal and transverse ρ-production amplitudes.

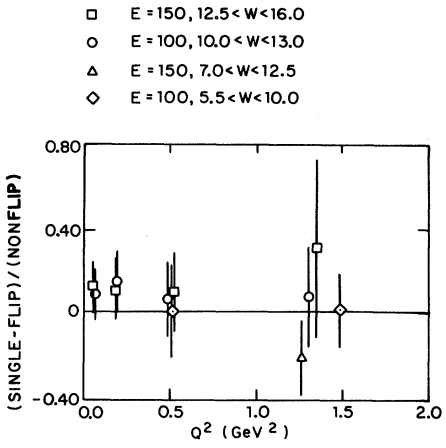

FIG. 18. The ratio of ρ helicity-single-flip to helicity-nonflip amplitudes.

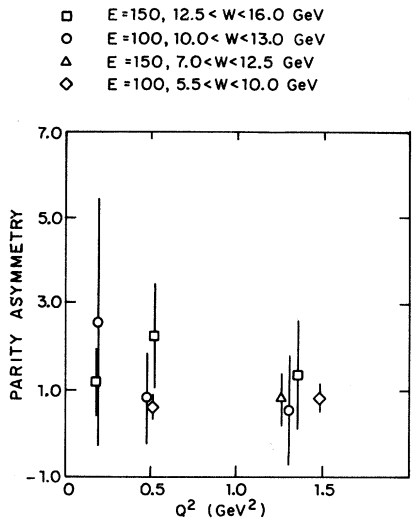

FIG. 19. ρ production parity asymmetry parameter.

D. Exclusive four-pion results

The distribution of the difference between the square of the mass of the recoil nucleon and the square of the target-proton mass for four-particle neutral final states shows an elastic peak which, like the distribution for two-particle final states, is enhanced if events with $-t$ greater than 0.8 GeV^2 or interaction vertex outside of the target are excluded (Fig. 20). We consider events with muon class 3 or less, hadron class 2 or less, apparatus trigger produced by the detected particles (as opposed to randoms), and interaction vertex within three standard deviations of the target. If the downstream particles are presumed to be pions their invariant-mass distribution peaks at around 1600 MeV and has a width of approximately 400 MeV (Fig. 21). A four-pion resonance with these values has previously been observed both in e^+e^- annihilation[36–38] and in photoproduction on hydrogen,[39,40] on deuterium,[41] and on carbon.[42]

The identification of this resonance with a vector meson, the ρ' (1600), seems more than plausible. The distribution in t of four-pion elastic events (without acceptance corrections, which should have little effect on this distribution) is exponential, with a slope for $-t$ less than 0.8 GeV^2 of 5.2±0.7 at 150 GeV and 5.2±1.0 at 100 GeV (Fig. 22). This can be compared with the slopes for the ρ of 8.3±0.2 and 6.6±0.2, and for the ϕ of 7.2±2.5 and 4.8±2.2, measured at 150 and 100 GeV. In light of the small number of four-pion elastic events available from this experiment, the task of rigorously calculating acceptance and applying corrections was not undertaken. The raw (uncorrected) ratio of observed four-pion elastic events to two-hadron elastic events is 0.13±0.02 at 150 GeV and 0.06±0.01 at 100 GeV. A measurement of production of the ρ' (1600) state by 17.5-GeV photons on deuterium has yielded a ρ' (1600)-to-ρ ratio of 0.06±0.01 for charged-pion decay modes.[41]

TABLE VII. ρ density-matrix elements, 150-GeV data. $0<Q^2<3$ GeV^2. $12.5<W<16.0$ GeV. $\langle\epsilon\rangle=0.37$.

	Element					
	00	11	Re10	Im10	1-1	Im1-1
Matrix						
04	0.07±0.04		0.07±0.03		−0.07±0.04	
1	−0.08±0.94	0.06±0.74	0.02±0.36		1.04±0.57	
2				0.05±0.28		−0.15±0.74
$P\times3$				−0.01±0.03		−0.05±0.05
5	0.04±0.09	−0.04±0.09	0.09±0.04		0.02±0.08	
6				−0.17±0.04		0.02±0.08
$P\times7$				0.01±0.05		0.01±0.09
$P\times8$	0.08±0.13	−0.06±0.11	0.04±0.05		−0.03±0.10	

$R=0.13\pm0.07$,
SCHC $\chi^2=17.2$ for 19 degrees of freedom
(single flip)/(nonflip)$=0.14\pm0.08$
$\cos\delta=1.07\pm0.24$
$P\sin\delta=0.17\pm0.29$.

TABLE VIII. ρ density-matrix elements, 100-GeV data. $0<Q^2<3$ GeV^2. $10.0<W<13.0$ GeV. $\langle\epsilon\rangle=0.40$.

	Element					
	00	11	Re10	Im10	1-1	Im1-1
Matrix						
04	0.05±0.03		0.06±0.03		−0.06±0.04	
1	0.72±1.80	−1.15±2.42	0.45±0.78		1.20±0.48	
2				0.34±0.41		−0.95±0.84
$P\times3$				−0.01±0.03		−0.06±0.05
5	0.07±0.10	−0.13±0.10	0.15±0.05		0.03±0.07	
6				−0.07±0.05		−0.19±0.09
$P\times7$				−0.01±0.06		−0.16±0.14
$P\times8$	−0.12±0.12	0.10±0.12	−0.03±0.06		0.03±0.10	

$R=0.10\pm0.07$
SCHC $\chi^2=20.0$ for 19 degrees of freedom
(single flip)/(nonflip)$=0.11\pm0.08$
$\cos\delta=1.09\pm0.34$
$P\sin\delta=0.18\pm0.38$

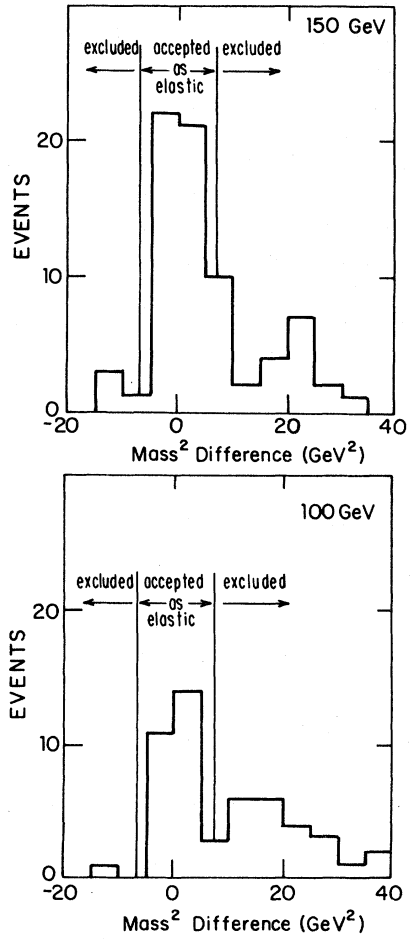

FIG. 20. Difference between the square of the recoil-nucleon missing mass and the square of the proton mass, for four-particle events with $-t$ less than 0.8 GeV^2 passing the vertex cut.

VI. CONCLUSION

We have measured diffractive muoproduction of ρ, ϕ, and ρ' (1600) mesons from a proton target

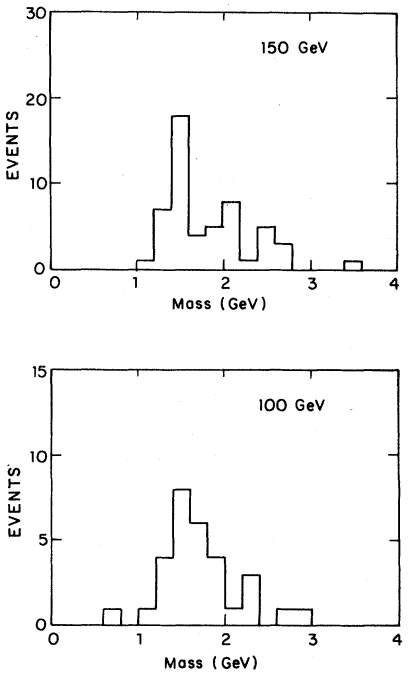

FIG. 21. Invariant mass of four-pion final states.

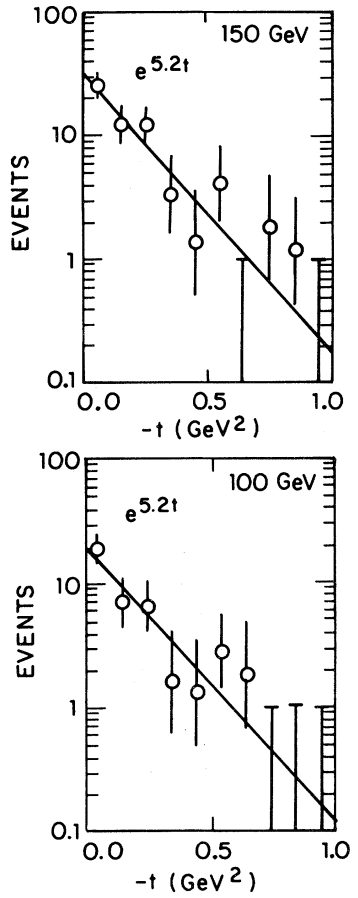

FIG. 22. Uncorrected t distribution for four-pion events.

with beam energies of 150 and 100 GeV. The ρ-production process is consistent with the predictions of the vector-dominance model, and shows little contribution from longitudinal ρ production. The ρ mass distribution is skewed, and s-channel helicity is largely conserved, although we do detect a small helicity-single-flip contribution. All three processes have distributions in t which fall exponentially with increasing t.

ACKNOWLEDGMENTS

We would like to thank the many people whose assistance made this experiment possible, in particular, R. Burns, R. Haggerty, J. O'Kane, E. Sadowski, and H. Weedon at Harvard; R. Armstrong, K. Burns, R. Gabriel, B. Grumman, W. Nakagawa, B. Norton, T. Nunamaker, F. Quinn, and D. Turner at the Enrico Fermi Institute; P. Burton, L. Jones, and J. MacAllister at Oxford; E. W. G. Wallis and his staff at the Rutherford Laboratory; and the Neutrino crews at the Fermi National Accelerator Laboratory. This research was supported by the U. S. Energy Research and Development Administration, the U. S. Department of Energy, the National Science Foundation, and the Science Research Council (United Kingdom).

---

*Present address: Department of Physics, Northeastern University, Boston, Mass. 02115.

†Present address: Science Applications, Inc., McLean, Va. 22102.

‡Present address: Fermi National Accelerator Laboratory, Batavia, Ill. 60510.

§Present address: Massachusetts General Hospital, Boston, Mass. 02125.

||Present address: Teledyne Brown Engineering, Huntsville, Ala. 35807.

¶Present address: Los Alamos Scientific Laboratory, Los Alamos, N. M. 87545.

**Present address: Department of Physics, Virginia Polytechnic Institute, Blacksburg, Va. 20461.

††Present address: Bell Laboratories, Naperville, Ill. 60540.

‡‡Present address: Department of Physics and Astronomy, Vanderbilt University, Nashville, Tenn. 37235.

§§Present address: Department of Physics, University of California, Santa Barbara, Calif. 93106.

||||Present address: Hansen Laboratory, Stanford University, Stanford, Calif. 94305.

¶¶Present address: CRA Services, Ltd., Melbourne, Victoria, Australia.

***Present address: Department of Physics and Astronomy, University of Maryland, College Park, Md. 20742.

[1]W. R. Francis, H. L. Anderson, V. K. Bharadwaj, N. E. Booth, R. M. Fine, B. A. Gordon, R. H. Heisterberg, R. G. Hicks, T. B. W. Kirk, G. I. Kirkbride, W. A. Loomis, H. S. Matis, L. W. Mo, L. C. Myrianthopoulos, F. M. Pipkin, S. H. Pordes, T. W. Quirk, W. D. Shambroom, A. Skuja, L. J. Verhey, W. S. C. Williams, Richard Wilson, and S. C. Wright, Phys. Rev. Lett. 38, 633 (1977).

[2]Y. Nambu, Phys. Rev. 106, 1366 (1957).

[3]M. Ross and L. Stodolsky, Phys. Rev. 149, 1172 (1966).

[4]J. Ballam, G. B. Chadwick, R. Gearhart, Z. G. T. Guiragossian, J. J. Murray, P. Seyboth, C. K. Sinclair,

I. O. Skillicorn, H. Spitzer, G. Wolf, H. H. Bingham, W. B. Fretter, K. C. Moffeit, W. J. Podolsky, M. S. Rabin, A. H. Rosenfeld, R. Windmolders, and R. H. Milburn, Phys. Rev. D 5, 545 (1972).

[5]J. Ballam, G. B. Chadwick, Y. Eisenberg, E. Kogan, K. C. Moffeit, P. Seyboth, I. O. Skillicorn, H. Spitzer, G. Wolf, H. H. Bingham, W. B. Fretter, W. J. Podolsky, M. S. Rabin, A. H. Rosenfeld, and G. Smadja, Phys. Rev. D 7, 3150 (1973).

[6]H. Fraas and D. Schildknecht, Nucl. Phys. B14, 543 (1969).

[7]C. F. Cho and G. J. Gounaris, Phys. Rev. 186, 1619 (1969).

[8]C. Driver, K. Heinloth, K. Hohne, G. Ofmann, F. Janata, P. Karow, D. Scmidt, G. Spect, and J. Rathje, Nucl. Phys. B38, 1 (1972).

[9]V. Eckardt, H. J. Gebauer, P. Joos, H. Meyer, B. Naroska, D. Notz, W. J. Podolsky, G. Wolf, S. Yellin, G. Drews, H. Nagel, and E. Rabe, Phys. Lett. 43B, 240 (1973).

[10]V. Eckardt, H. J. Bebauer, P. Joos, H. Meyer, B. Noraska, D. Notz, W. J. Podolsky, G. Wolf, S. Yellin, H. Dau, G. Drews, D. Greubel, W. Meincke, H. Nagel, and E. Rabe, Nucl. Phys. B55, 45 (1973).

[11]P. Joos, A. Ladage, H. Meyer, P. Stein, G. Wolf, S. Yellin, C. K. Chen, J. Knowles, D. Martin, J. M. Scarr, I. O. Skillicorn, K. Smith, C. Benz, G. Drews, D. Hoffmann, J. Knobloch, W. Kraus, H. Nagel, E. Rabe, C. Sander, W. D. Schlatter, H. Spitzer, and K. Wacker, Nucl. Phys. B113, 53 (1976).

[12]D. E. Andrews, K. Berkelman, D. G. Cassel, D. L. Hartill, J. Hartmann, R. Kerchner, E. Lazarus, R. M. Lettauer, R. L. Loveless, R. Rohlfs, D. H. White, and A. J. Sadoff, Phys. Rev. Lett. 26, 864 (1971).

[13]E. D. Bloom, R. L. A. Cottrell, H. DeStaebler, C. L. Jordan, G. Miller, H. Piel, C. Prescott, R. Siemann, C. K. Sinclair, S. Stein, and R. E. Taylor, Phys. Rev. Lett. 28, 516 (1972).

[14]L. Ahrens, K. Berkelman, G. S. Brown, D. G. Cassel, W. R. Francis, P. H. Barbincius, D. Harding, D. L. Hartrill, J. L. Hartmann, R. L. Loveless, R. C. Rohlfs, D. H. White, and A. J. Sadoff, Phys. Rev. Lett. 31, 131 (1973).

[15]L. Ahrens, K. Berkelman, G. S. Brown, D. G. Cassel, W. R. Francis, P. H. Barbinicius, D. Harding, D. L. Hartrill, J. L. Hartmann, R. L. Loveless, R. C. Rohlfs, D. H. White, and A. J. Sadoff, Phys. Rev. D 9, 1894 (1974).

[16]L. A. Ahrens, K. Berkelman, D. G. Cassel, C. T. Day, B. G. Gibbard, D. J. Harding, D. L. Hartill, J. W. Humphrey, T. J. Killian, D. S. Klinger, J. T. Linnemann, E. A. Treadwell, and D. H. White, Phys. Rev. Lett. 42, 208 (1974).

[17]J. T. Dakin, G. J. Feldman, W. L. Lakin, F. Martin, M. L. Perl, E. W. Petraske, and W. T. Toner, Phys. Rev. Lett. 30, 142 (1973).

[18]J. T. Dakin, G. J. Feldman, W. L. Lakin, F. Martin, M. L. Perl, E. W. Petraske, and W. T. Toner, Phys. Rev. D 8, 687 (1973).

[19]J. Ballam, E. D. Bloom, J. T. Carroll, G. B. Chadwich, R. L. A. Cottrell, M. Della Negra, H. DeStaebler, I. K. Gershwin, L. P. Keller, M. D. Mestayer, K. C. Moffeit, C. Y. Prescott, and S. Stein, Phys. Rev. D 10, 765 (1974).

[20]C. del Papa, D. Dorfan, S. M. Flatte, A. Grillo, C. A. Heusch, B. Liberman, L. Moss, T. Schalk, A. Seiden, K. Bunnell, M. Duong-van, R. Mozley, A. Odian, F. Villa, and L. C. Wang, Phys. Rev. D 19, 1303 (1979).

[21]R. Dixon, R. Galik, M. Herzlinger, S. D. Holmes, D. Larson, F. M. Pipkin, S. Raither, A. Silverman, and R. L. Wagner, Phys. Rev. Lett. 39, 516 (1977).

[22]T. H. Bauer, R. D. Spital, D. R. Yennie, and F. M. Pipkin, Rev. Mod. Phys. 50, 261 (1978).

[23]L. N. Hand, Phys. Rev. 129, 1834 (1963).

[24]K. Schilling and G. Wolf, Nucl. Phys. B61, 381 (1973).

[25]W. A. Loomis, B. A. Gordon, F. M. Pipkin, S. H. Pordes, W. D. Shambroom, L. J. Verhey, Richard Wilson, H. L. Anderson, R. M. Fine, R. H. Heisterberg, H. S. Matis, L. Mo, L. C. Myrianthopoulos, S. C. Wright, W. R. Francis, R. G. Hicks, T. B. W. Kirk, V. K. Bharadwaj, N. E. Booth, G. I. Kirkbride, T. W. Quirk, A. Skuja, M. A. Staton, and W. S. C. Williams, Phys. Rev. D 19, 2543 (1979).

[26]B. A. Gordon, W. A. Loomis, F. M. Pipkin, S. H. Pordes, A. L. Sessoms, W. D. Shambroom, C. Tao, L. J. Verhey, Richard Wilson, H. L. Anderson, R. M. Fine, R. H. Heisterberg, W. W. Kinnison, H. S. Matis, L. W. Mo, L. C. Myrianthopoulos, S. C. Wright, W. R. Francis, R. G. Hicks, T. B. W. Kirk, T. W. Quirk, V. K. Bharadwaj, N. E. Booth, G. I. Kirkbride, J. Proudfoot, A. Skuja, M. A. Staton, and W. S. C. Williams, Phys. Rev. D 20, 2645 (1979).

[27]J. M. Hammersley and D. C. Handscomb, *Monte Carlo Methods* (Methuen, London, 1964).

[28]P. Urban, *Topics in Applied Quantum Electrodynamics* (Springer, New York, 1970).

[29]L. W. Mo and Y. S. Tasai, Rev. Mod. Phys. 41, 205 (1969).

[30]P. Soding, Phys. Rev. Lett. 19, 702 (1966).

[31]G. Kramer and H. R. Quinn, Nucl. Phys. B27, 77 (1971).

[32]R. Spital and D. R. Yennie, Phys. Rev. D 9, 126 (1974).

[33]J. D. Jackson, Nuovo Cimento 34, 1644 (1964).

[34]R. M. Egloff, P. J. Davis, G. J. Luste, J. F. Martin, J. D. Prentice, D. O. Caldwell, J. P. Cumalat, A. M. Eisner, A. Lu, R. J. Morrison, S. J. Yellin, and T. Nash, Phys. Rev. Lett. 43, 657 (1979).

[35]A. R. Clark, K. J. Johnson, L. T. Kerth, S. C. Loken, T. W. Markiewixz, P. D. Meyers, W. J. Smith, M. Strovink, W. A. Wenzel, R. P. Johnson, C. Moore, M. Mugge, R. E. Shafer, G. D. Gollin, F. C. Shoemaker, and P. Surko, Phys. Rev. Lett. 43, 187 (1979).

[36]G. Barbarino, M. Gilli, E. Iarocci, P. Spillantini, V. Valente, R. Visentin, F. Ceradini, M. Conversi, L.

Paoluze, R. Santonico, M. Nigro, L. Trasatti, and G. T. Zorn, Lett. Nuovo Cimento 3, 689 (1972).

[37]M. Gilli, E. Iarocci, P. Spillantini, V. Valente, R. Visentin, B. Borgia, F. Ceradini, M. Conversi, L. Paoluzi, R. Santonico, M. Nigro, L. Trasatti, and G. T. Zorn, Nuovo Cimento 13A, 593 (1973).

[38]M. Conversi, L. Paoluzi, F. Ceradini, S. d'Angelo, M. L. Ferrer, R. Santonico, M. Grilli, P. Spillantini, and V. Valente, Phys. Lett. 52B, 493 (1974).

[39]H. H. Bingham, W. B. Fretter, W. J. Podolsky, M. S. Rabin, A. H. Rosenfeld, G. Smadja, G. P. Yost, J. Ballam, G. B. Chadwick, Y. Eisenberg, E. Kogan, K. C. Moffeit, P. Seyboth, I. O. Skillicorn, H. Spitzer, and G. Wolf, Phys. Lett. 41B, 635 (1972).

[40]M. Davier, I. Derado, D. E. C. Fries, F. F. Liu, R. F. Mozley, O. Odian, J. Park, W. P. Swanson, F. Villa, and D. Yount, Nucl. Phys. B58, 31 (1973).

[41]G. Alexander, O. Benary, J. Gandsman, D. Lissauer, A. Levy, Y. Oren, and L. M. Rosenstein, Phys. Lett. 57B, 487 (1975).

[42]M. S. Atiya, S. D. Holmes, B. C. Knapp, W. Lee, R. Seto, W. J. Wisniewski, P. Avery, J. Butler, G. Gladding, M. C. Goodman, T. O'Halloran, J. J. Russell, A. Wattenberg, J. Wiss, M. Binkley, J. P. Cumulat, I. Gaines, M. Gormley, R. L. Loveless, and J. Peoples, Phys. Rev. Lett. 43, 1691 (1979).